IOP Publishing Nanotechnology
Nanotechnology 29 (2018) 135202 (9pp) https://doi.org/10.1088/1361-6528/aaaaef

# Polarized emission from $CsPbBr_3$ nanowire embedded-electrospun PU fibers

**Tuğrul Güner[1], Gökhan Topçu[1], Umut Savacı[2], Aziz Genç[3], Servet Turan[2], Emre Sari[4,5] and Mustafa M Demir[1,5]**

[1] Department of Materials Science and Engineering, Izmir Institute of Technology, Izmir, Turkey
[2] Department of Materials Science and Engineering, Anadolu University, Eskişehir, Turkey
[3] Department of Metallurgy and Materials Engineering Bartın University, Bartın, Turkey
[4] Department of Photonics, Izmir Institute of Technology, Izmir, Turkey

E-mail: emresari@iyte.edu.tr and mdemir@iyte.edu.tr

Received 18 December 2017, revised 24 January 2018
Accepted for publication 29 January 2018
Published 14 February 2018

**Abstract**

Interest in all-inorganic halide perovskites has been increasing dramatically due to their high quantum yield, band gap tunability, and ease of fabrication in compositional and geometric diversity. In this study, we synthesized several hundreds of nanometer long and ~4 nm thick $CsPbBr_3$ nanowires (NWs). They were then integrated into electrospun polyurethane (PU) fibers to examine the polarization behavior of the composite fiber assembly. Aligned electrospun fibers containing $CsPbBr_3$ NWs showed a remarkable increase in the degree of polarization from 0.17–0.30. This combination of NWs and PU fibers provides a promising composite material for various applications such as optoelectronic devices and solar cells.

Keywords: alignment, electrospinning, nanocomposite, perovskite, photoluminescence

(Some figures may appear in colour only in the online journal)

## 1. Introduction

All-inorganic halide perovskites have attracted significant attention in recent years due to their unique optical properties [1]. In addition to their intrinsic stability compared to organometallic halide perovskites [2, 3], these nanocrystals (NCs) exhibit bright and ultra-high photoluminescence (PL) quantum yield (90%) [4, 5], narrow band emission [2, 5], and wavelength tunability through size and composition [4, 6–10]. These optical characteristics of the all-inorganic perovskite NCs have led to different types of applications including optoelectronic devices and optical components such as lasers [11–14] and LEDs [2, 15–17].

Polarized light is an electromagnetic wave composed of an electric field that propagates in a particular plane. Polarization of an incoherent light source is characterized by the degree of polarization $P$ that can theoretically take a value between 0 (unpolarized) and 1 (polarized):

$$P = \frac{I_{max} - I_{min}}{I_{max} + I_{min}}, \quad (1)$$

where $I$ refers to the PL intensity of the light source that is collected after passing through the polarizer. Polarization is utilized in many fields including displays, telecommunications, information storage, and ultra-sensitive photodetectors, etc [18]. Recently, Wang *et al* investigated the polarization characteristics of all-inorganic perovskite $CsPbBr_xI_{(3-x)}$ NCs [19]. These NCs were observed to have a strong degree of polarization up to 0.36 in solution and 0.40 in film for a particular Br/I composition. However, the polarized emission from these NCs was obtained from only a single crystal cubic phase of $CsPbBr_xI_{(3-x)}$. There are well-known morphologies of this crystal such as nanoplatelets [20], nanowires (NWs) [7, 21, 22], and nanosheets [23], which may show the potential of further enhancements in the degree of polarization of these NCs [24–26].

Electrospinning is a process that can produce nano- to micro-scaled fibers in diameter via the high potential difference between the nozzle of a solution container and a grounded and conductive collector [27]. It is a facile and inexpensive process to obtain nanosized polymeric and composite fibers. Moreover, it provides full control of the morphology of individual fibers (fiber diameter, shape, and

[5] Authors to whom any correspondence should be addressed.

 

surface chemistry). The fibers are formed through a jet that occurs from the electrostatically charged surface of a polymer droplet to the grounded collector. These electrospun fibers are often collected as randomly oriented structures in the form of nonwoven mats [27]. Since their disordered structures are not convenient for use in device fabrications (i.e. microelectronics and photonics) due to the scattering of light, well-aligned and highly ordered architectures are often desired to have obtain coherent interaction of light with the structures. For instance, the alignment of the fiber assembly can yield a polarized luminescence or can even enhance it [28–30]. In order to obtain aligned fibers, several methods, for instance employing parallel positioned metal strips with an air gap [31] or a rotating drum as collector [32], have been reported in the literature. Apart from the electrospinning technique, the ordered array of indefinitely long NW fibers was achieved via a new iterative size-reduction process [33] or a sonochemical approach can be used to achieve single crystal NW composite fibers [34]. Electrospinning provides not only a way to obtain uniaxial fibers but also can be used to align nanostructures [35–37]. The ability to achieve such a type of hierarchical nanocomposites is a facile way to produce advanced optical materials. The alignment of the fibers provides a 1D hierarchical structure that can potentially be used in a polarization filter [37].

In this study, $CsPbBr_3$ NWs were prepared and integrated with polymeric film prepared by solution electrospinning and film casting. The fibers were spun from solution in both a nonwoven and an aligned arrangement. This aligned composite fiber assembly was found to exhibit polarization higher than that of the NW dispersion. Moreover, it showed a higher level compared to that of both the drop-cast film and the randomly positioned nonwoven fibers. This approach of composite fabrication is simple, flexible, and customizable; therefore, it can be readily used in future optoelectronic applications based on 1D materials.

## 2. Experimental

### 2.1. Materials

Cesium carbonate ($Cs_2CO_3$, 99.9%, Sigma-Aldrich), lead(II) bromide ($PbBr_2$, ⩾98%, Sigma-Aldrich), oleic acid (OA, 90%, Alfa Aesar), oleylamine (OLA, 90%, Sigma-Aldrich), 1-octadecene (ODE, 90%, Sigma-Aldrich), dimethylformamide (DMF, ⩾99.9%, Tekkim), acetone (Merck, ⩾99.5%), dichloromethane (DCM, ⩾99.9%, Sigma-Aldrich), tetrahydrofuran (THF, VWR, ⩾99.7%), and polyurethane (PU, Ravago) were purchased and used as received without any further purification.

### 2.2. Methods

The diffraction profile of the $CsPbBr_3$ NWs was recorded with an x-ray diffractometer (X'Pert Pro, Philips, Eindhoven, the Netherlands). High resolution transmission electron microscopy (HRTEM; JEOL 2100F, operated at 200 kV) was employed to examine the NW morphology. Scanning electron microscopy (SEM; Quanta 250, FEI, Hillsboro, OR, USA) was used to determine the NW embedded-electrospun fiber morphology with both back-scattering electron (BSE) and scanning transmission electron microscope (STEM) detectors. The time resolved and polarized emission spectra of both the NWs and NW embedded fibers were recorded on an FS5 Spectrofluorometer (Edinburgh Instruments, UK).

### 2.3. Synthesis of Cs-oleate

The Cs-oleate solution was synthesized by following the procedure used by Amgar *et al* [7]. $Cs_2CO_3$ (0.2 g), OA (625 $\mu$l), and ODE (7.5 ml) were loaded into a three necked flask, and dried under vacuum (150 mbar) at 120 °C for 1 h. Subsequently, the mixture was heated to 150 °C under $N_2$, and the reaction was maintained until all the $Cs_2CO_3$ was consumed by OA. Afterwards, the yellowish Cs-oleate solution was gradually cooled down (it had to be pre-heated to 100 °C before using).

### 2.4. Synthesis of $CsPbBr_3$ NWs

$CsPbBr_3$ NWs were prepared in four steps with slight modifications based on the procedure in [7]. First, aliquots of 0.125 ml of OA, 0.125 ml of OLA, and 1.25 ml of ODE were loaded into a glass vial. Second, 0.1 ml of pre-heated Cs-oleate solution was added to the mixture subsequently. The third step involved the addition of 0.2 ml of $PbBr_2$ precursor solution (0.4 M, heated for 1 h at 80 °C until full dissolution). Fourth, 5 ml of acetone were rapidly added to trigger the crystallization of the $CsPbBr_3$ NWs. Stirring was maintained for 30 min and green precipitates were collected by using centrifuge (6000 rpm, 10 m). The precipitates were re-dispersed in DCM.

### 2.5. Preparation of $CsPbBr_3$ NW embedded fibers

$CsPbBr_3$ NW embedded PU fibers were prepared by electrospinning. Two parallel steel strips were placed 5 mm apart from each other on an aluminum foil collector to obtain aligned fibers. The electrospinning of a suspension of NWs and PU solution (25 wt.% in THF) was used to form composite fibers. The solid content of the NWs was fixed to 0.15 wt.% with respect to the polymer. Aliquots of 5 ml of PU solution, 0.3 ml of THF, and 0.3 ml of NW/DCM dispersion were mixed in a glass vial, and then the resulting suspension was loaded into a syringe. Two electrode holders were connected to the syringe needle and the collector, respectively. A fixed potential of 15 kV was applied and the flow rate was set to 0.8 ml $h^{-1}$.

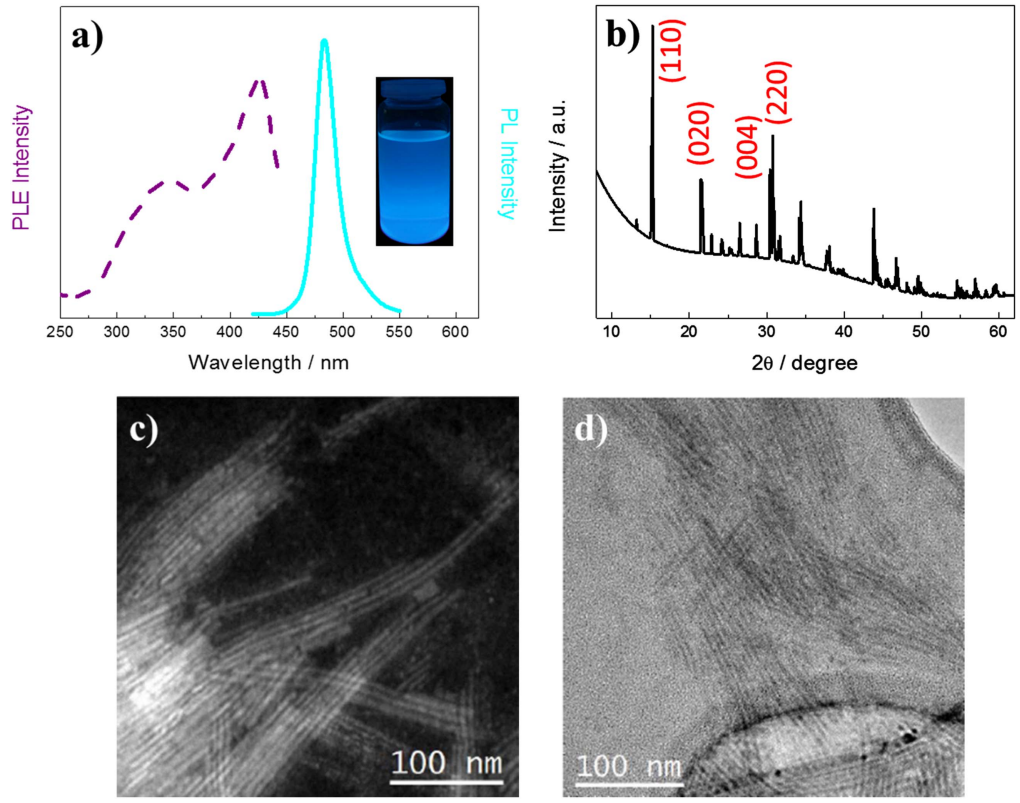


**Figure 1.** (a) PLE ($\lambda_{em}$: 490 nm) and PL ($\lambda_{ex}$: 400 nm) spectra of the $CsPbBr_3$ NWs and the inset shows a photograph of the NW dispersion in DCM under UV light (366 nm), (b) x-ray diffraction of $CsPbBr_3$ indicating the crystallographic features of the NWs. (c), (d) HAADF STEM and TEM images of the NWs cast from DCM dispersion showing a uniform thickness of 4 nm.

## 3. Results and discussion

### *3.1. Synthesis of NW and preparation of composite electrospun fibers*

The $CsPbBr_3$ NWs were examined using the spectroscopy, diffraction, and microscopy techniques. Figure 1(a) shows the photoluminescence excitation (PLE) and emission spectra of the NW samples dispersed in DCM. The violet dashed line denotes the excitation spectra recorded at an emission wavelength of 490 nm, and covered a wide range of 250 to ~450 nm. For the emission spectrum, the NWs were excited at the wavelength of 400 nm, and a single narrow emission (FWHM = 23 nm) at 490 nm was observed. This excitonic narrow blue emission may be the result of a quantum confinement effect due to the narrow diameter of the wire [21]. Although the dispersion of particles in DCM is yellowish green under daylight, they showed a strong blue emission under UV (inset of figure 1(a)).

The XRD pattern of the NWs is presented in figure 1(b). The characteristic reflections at 15° and 22° correspond to the planes (110) and (020), respectively. Moreover, two sharp reflections at ~30° and ~31° represent the planes (004) and (220). These signals verify the standard orthorhombic pattern of $CsPbBr_3$ [38]. Figures 1(c) and (d) show several low magnification high angle annular dark field (HAADF) STEM and TEM images revealing that the sample mostly consists of 4 nm thick and several hundreds of nanometer long NWs. Most of these NWs were present as bundles, as clearly shown in the HAADF STEM image, yet it was possible to observe individually dispersed NWs. This finding verifies the formation of 1D anisotropic growth of $CsPbBr_3$. This type of growth may be achieved via anisotropic interfacial energy of different crystal planes those are covered and passivated by OA and OLA, respectively [7, 34]. In the following, we present some detailed HRTEM investigations of the structure and phase of these NWs. Unfortunately, due to the instability of the structure under electron beam, relatively larger structures are used for the examinations. Figure 2 shows a HRTEM micrograph of the nanostructures with various thicknesses (6 and 27 nm). The details of the red squared area from the tip of the wider nanostructure and its related power spectrum obtained by fast Fourier transform (FFT) are presented in this figure. The FFT shown on the right indicates that this nanostructure is composed of an orthorhombic $CsPbBr_3$ phase (space group = Pnma) with lattice parameters of $a = 0.82$ nm, $b = 1.17$ nm, and $c = 0.82$ nm and it is visualized along its [−110] zone axis. Then again, the tip of a ~6 nm thick NW (indicated by a green square) is found out to be crystalline and as indicated in its detailed image, the present lattice fringes belong to the {004} family of planes of the same orthorhombic $CsPbBr_3$ phase.

$CsPbBr_3$ nanocrystals are extremely sensitive materials against a polar environment [39]. This sensitive nature can be attributed to the highly ionic structure of the nanocrystals and dynamic ligand coverage onto their surface. Therefore, the

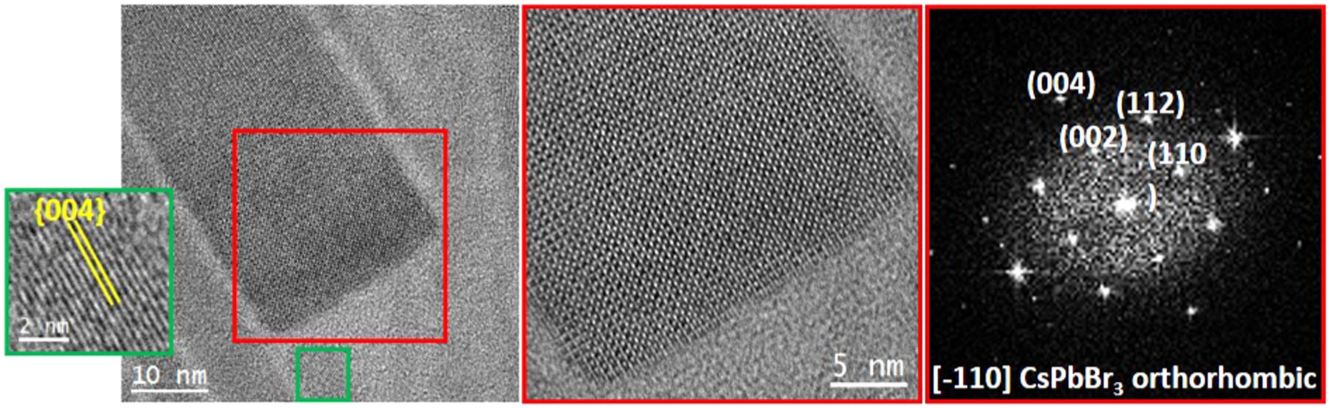


**Figure 2.** HRTEM image showing several nanostructures with various thicknesses (6 and 27 nm). The red squared figures indicate the lattice fringes and the corresponding power spectra of the thicker samples whereas the green square shows the lattice fringes of the 6 nm one.

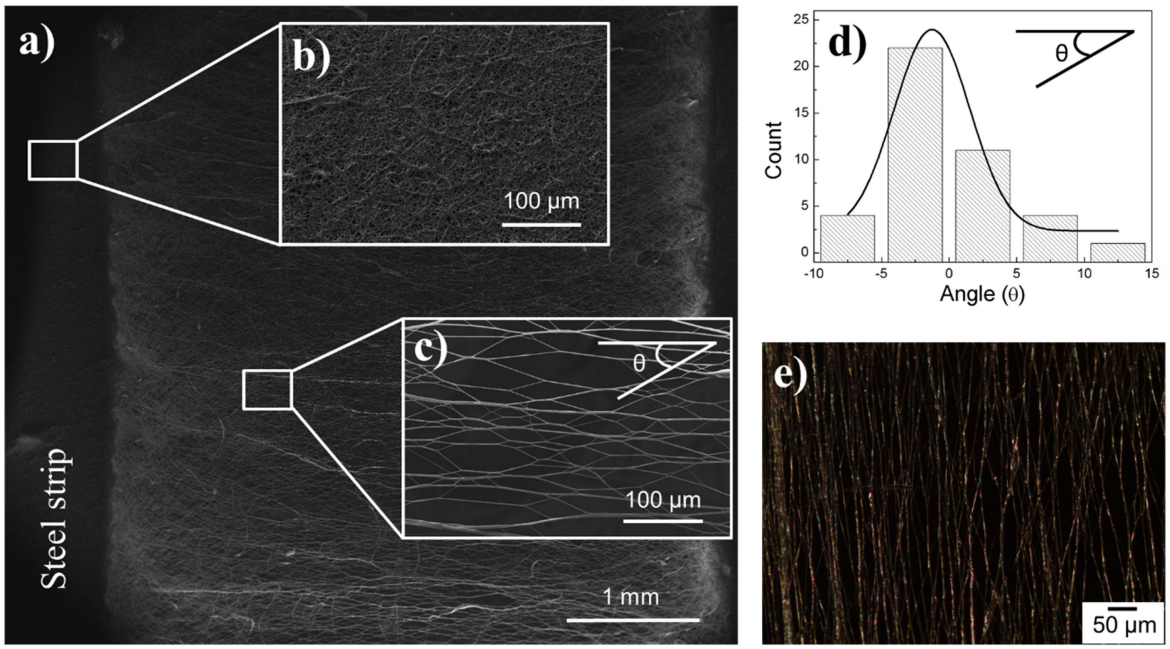


**Figure 3.** (a) SEM images of NW embedded fibers in several magnifications. The white squared ones show (b) randomly deposited electrospun fibers collected over the surface of steel strips and (c) aligned fibers uniaxially formed across the gap between the strips. (d) Population of fibers at various angles ($\theta$) towards one another showing the degree of alignment whereas $\theta$ defines the angle between the direction of the fiber and the normal steel strips. (e) Optical microscopy image of fibers also showing the alignment.

integration of these nanostructures into a polymer matrix via electrospinning is a process that should be carried out carefully. It needs to be overcome by using polar solvents. Figure 3 shows the morphology of the electrospun fibers containing NWs. In figure 3(a), SEM images of both the aligned and nonwoven fibers are shown in the air gaps between the strips and on the strips, respectively. The nonwoven fibers developed on the steel strips show an intensive fiber distribution and random alignment (figure 3(b)). On the other hand, the aligned fibers between the steel strips are formed in an assembly without sticking to each other. Moreover, these fibers possess an ordered 1D arrangement between the steel strips. These fibers are examined by measuring the degree of alignment using the ImageJ software on the SEM images. Following the axis and angle defined in figures 3(c) and (d), the result of the degree of alignment shows that these fibers are almost perfectly aligned with an angle very close to 0°. For a wide view of these aligned fibers, an optical microscope image is also given in figure 3(e). It is obvious that the fibers formed between these two steel strips show a very high degree of alignment. In other words, these aligned fibers are produced as having an explicit 1D arrangement.

A STEM image of the NW embedded-electrospun fibers is given figure 4(a). The fibers were found to be distributed without a preferential alignment over the copper mesh grids. As the inset of figure 4(a) shows, these NWs cover only small regions along the fiber having 0.5 $\mu$m diameter. Image of the nonwoven sample taken in the SEM backscatter mode is presented in figure 4(b). Bundles of NWs are evidently associated with the fibers. The NW bundles seem to be randomly distributed over the fiber volume. The shear rate

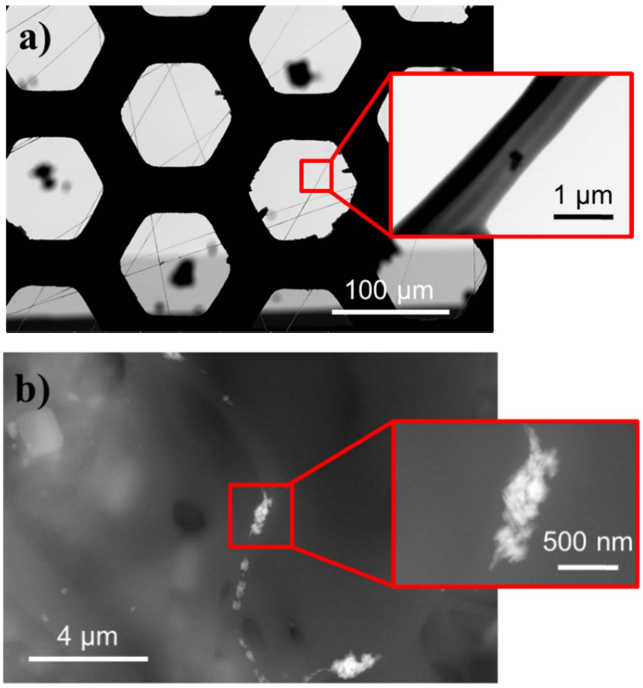


**Figure 4.** Representative NW embedded fiber images were also taken with (a) STEM and (b) BSE detectors. Red squared images showing NW bundle in PU fiber at a high magnification.

applied during the electrospinning process was able to orient the components of the precursor solution along the fiber axis [30, 37]. The aspect ratio of the wires is very high such that they bend, twist, and may undergo inter/intra wire entanglement. The size of the bundles (or aggregates) appears to be comparable with the diameter of the fibers so that the electrical force applied may not be able to orient them. The inset represents the focused backscatter image of the selected region, and the overview of this region explicitly demonstrates that this small region is composed of aggregated wires (where the geometry of the wire has already been verified by the TEM images shown in figure 1) forming NW aggregate. Attempts were made to image the alignment of the NWs in electrospun fiber volume via TEM. However, the fibers are not transparent under electron beam since the thickness of the individual fibers is around half a micron. The embedment of the fiber mat in epoxy resin for microtoming did not work due to the mechanical weakness of the submicron diameter PU fibers. They detached from the bulk epoxy matrix during the slicing process.

### *3.2. Optical features of $CsPbBr_3$ NWs and their electrospun PU composite fibers*

Polarization of NW/DCM dispersion was estimated through the PL spectra of NW/DCM dispersion in the presence of a polarizer (used as analyzer) at various angles (figure 5(a)). The PL intensity recorded at each angle from 0°–60° shows a systematic increase; however, a reduction is observed between 60°–150°. The difference in the angle between the maximum and minimum PL intensities ($I$) is 90° suggesting the resolution of parallel and perpendicular electrical fields,

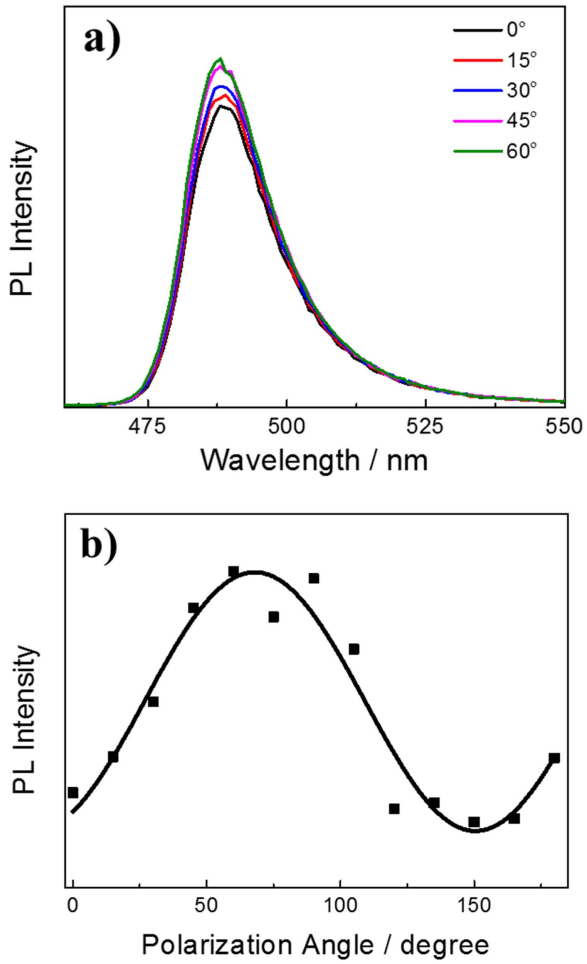


**Figure 5.** (a) PL spectra of the NWs with a polarizer between 0–60° and (b) the polarization properties of the $CsPbBr_3$ perovskite in DCM.

respectively. The degree of linear polarization can be obtained by using equation (1). The change in polarization with respect to the angle of the analyzer is explicitly demonstrated in figure 5(b). The data were fit using a sine function. Applying equation (1) to this set of data shows in a degree of linear polarization of 0.17. It is found to be higher than the polarization reported for $CsPbBr_3$ QDs (in the form of nanocubes) dispersed in hexane, which is approximately 0.075 [19]. The authors achieved enhancement of the polarization of $CsPbBr_3$ QDs by distorting the cubic structure of $CsPbBr_3$ through incorporating larger iodine atoms. Using this strategy, the authors were able to obtain a degree of linear polarization of 0.36 for $CsPbBr_xI_{(3-x)}$ in hexane. The reason for this significant increase was reported as due to breaking of the space inversion symmetry [19, 40]. The improvement observed in this study for the polarization of $CsPbBr_3$ was from 0.075 (QDs) to 0.17 (NWs). The reason may originate from the asymmetry of 1D wire geometry compared to the 0D nanocube.

Figure 6 shows the PL spectra of the prepared fibrous composite assembly. Compared to the emission spectra of the NW/DCM dispersion shown in figure 1(a), these samples showed a remarkable a redshift. The reason for this shift may

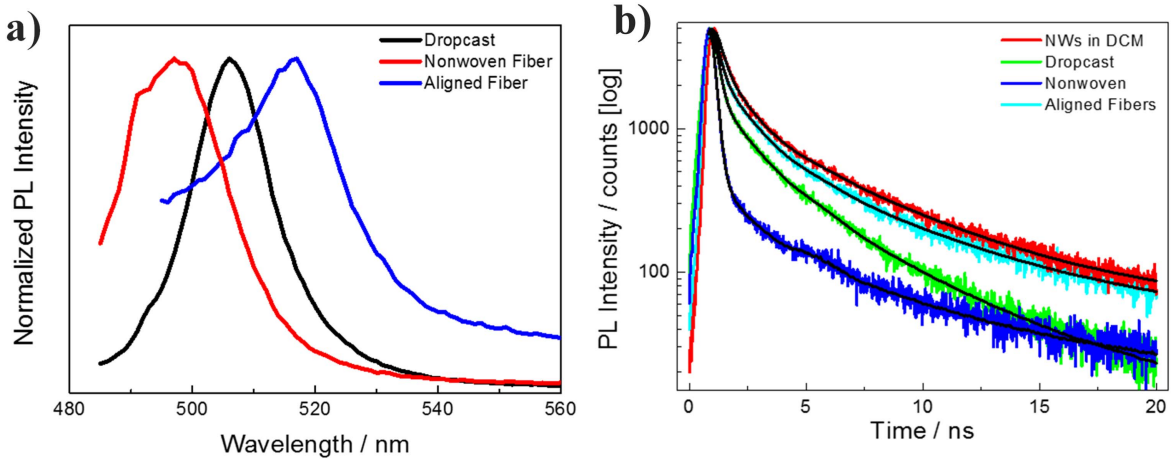


**Figure 6.** (a) PL spectra of the drop-cast film, electrospun nonwoven, and aligned fibers of the NWs and (b) time-resolved spectra of the DCM/$CsPbBr_3$ NW dispersion and their PU composites as drop-cast film, nonwoven, and aligned fibers showing their decay rates at their emission wavelengths ($\lambda$:490, 506, 497, and 517 nm), respectively.

**Table 1.** Multi-exponential fitting parameters of the time-resolved spectrum of the DCM/$CsPbBr_3$ NW dispersion, drop-cast film, nonwoven fibers, and aligned fibers.

| Sample | $\tau_1$(ns) | $A_1$(%) | $\tau_2$(ns) | $A_2$(%) | $\tau_3$(ns) | $A_3$(%) | $\tau_{ave}$(ns) |
|---|---|---|---|---|---|---|---|
| NWs in DCM | 0.23 | 18.26 | 1.12 | 28.34 | 5.22 | 53.40 | 3.15 |
| Drop cast | 0.14 | 35.51 | 1.45 | 28.64 | 4.75 | 35.85 | 2.17 |
| Nonwoven fiber | 0.01 | 51.38 | 1.40 | 12.42 | 6.15 | 36.20 | 2.41 |
| Aligned fiber | 0.17 | 23.45 | 1.34 | 32.30 | 5.68 | 44.25 | 2.99 |

be due to aggregation of $CsPbBr_3$ NWs forming bundles in the polymeric fiber or film [5, 41, 42]. The degree of redshift for the aligned and nonwoven fiber mats, and drop-cast film, was found to differ from each other. First, the PL of the nonwoven fibers shifted from 490–497 nm. Second, the PL of the drop-cast film is collected at 506 nm, while the one of the aligned fiber mats is collected at 517 nm. The reason for the difference in red-shifting between these samples, even though they possess the same composition, loading density, and surrounding matrix, may be the result of different NW bundle sizes developed in the course of structure formation. Self-absorption and/or Förster resonant energy transfer (FRET) between the smaller and larger NW bundles can also contribute to the PL shift [5, 41, 42]. On the other hand, highly asymmetric PL signals can be observed in figure 6. This result may also suggest the formation of bundles consisting of various numbers of individual NWs. Transient PL and the carrier lifetime characteristics of these samples are presented in figure 6(b) together with the NW/DCM dispersion. The wavelength at which photons are counted in lifetime measurements are chosen from their corresponding peak position of the PL spectra. All samples were fitted with tri-exponential decay (table 1 shows the details of these fittings parameters). The PL decay time, $\tau_1$, which is a fast decay process, may be related to charge carrier extraction either between NWs or their surrounding media. It was found that the averaged lifetime for NW/DCM is 3.15 ns. The decay times for the drop-cast film, nonwoven fibers, and aligned fibers are 2.17, 2.40, and 2.99 ns, respectively. The lifetime is reduced when the NWs are integrated into all solid polymeric films either obtained by casting or by electrospinning [43–45]. Unpassivation of perovskite surface via interaction with surrounding polymer chains and potential formation of new nonradiative decay pathways could be responsible for the reduction in lifetime ($\tau_1$). Nevertheless, they are comparable to each other implying that no significant change occurs in the presence of PU.

Polarizations of the all film samples including drop-cast film, nonwoven, and aligned fibrous mats are given in figure 7. It was found that the aligned fibers containing NWs showed polarization of nearly 0.30. Compared to the polarization of the NW/DCM dispersion, a 76% improvement was observed for the aligned NW/PU fiber mats. The enhancement may be achieved by partially orientated individual NWs along the aligned fiber axis in the fiber volume. Previously, Wang *et al* reported the polarization of $CsPbBr_3$ QDs in dispersion as 8%. The authors claimed that the polarization was destroyed upon their integration with the polymeric film (table 2). However, the polarization of NWs in all solid films/mats in this study is higher than their corresponding dispersion. The degree of linear polarization of nonwoven fibers was found to be 0.23, and the drop cast was 0.20. These values are worse than those for the aligned fibers. The degree of polarization of different samples including the $CsPbBr_3$ nanocubes [19] are summarized in table 2. Depending on the geometry, it is obvious that the prepared 1D asymmetric

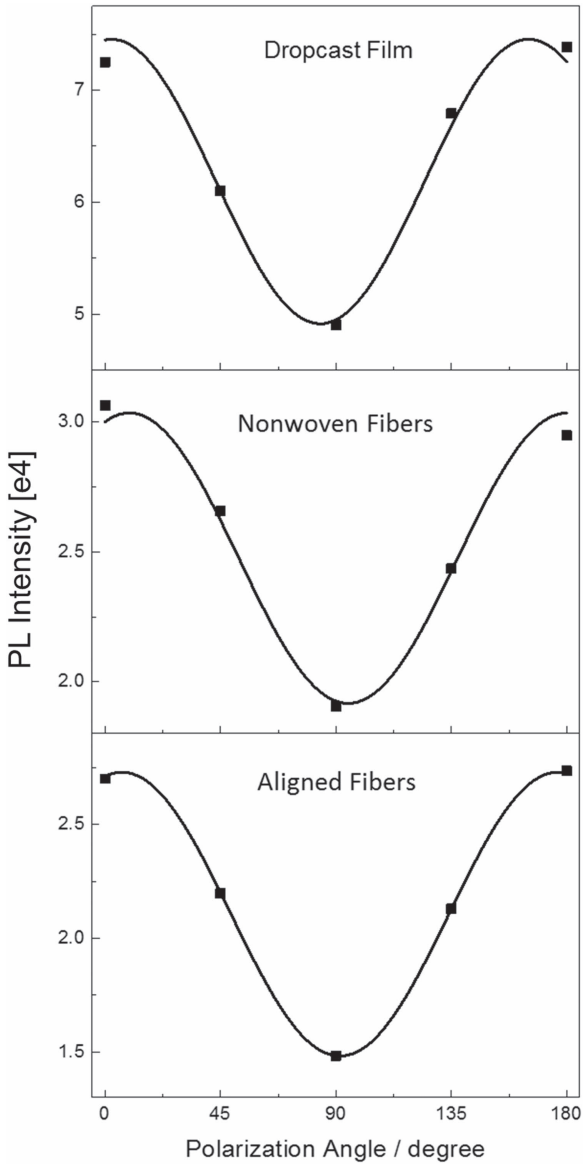


**Figure 7.** Polarization properties of drop-cast film, nonwoven, and aligned fibers of PU/$CsPbBr_3$ NW nanocomposites.

**Table 2.** Degree of polarization (%) of various samples including both the $CsPbBr_3$ NCs/hexane dispersion and $CsPbBr_3$ NC films reported by Wang *et al* [19] (first two data points) and the samples that were produced with NW geometry in PU (last four data points).

| Sample | Polarization (%) |
|---|---|
| $CsPbBr_3$ NCs in hexane | 8 |
| $CsPbBr_3$ NC film | 0.41 |
| $CsPbBr_3$ NWs in DCM | 17 |
| $CsPbBr_3$ NW drop-cast film | 20 |
| $CsPbBr_3$ NW nonwoven fibers | 23 |
| $CsPbBr_3$ NW aligned fibers | 30 |

$CsPbBr_3$ NWs showed enhancement compared to its 0D nanocube structure. Apart from this geometry based improvement, further enhancement for the degree of polarization is achieved via aligning the NW containing fibers.

## 4. Conclusion

$CsPbBr_3$ NWs with a width of ~4 nm and length of hundreds of nanometers were synthesized. The NWs were successfully integrated into electrospun PU fibers. The alignment of the fibers was achieved by simply changing the geometry of the electrospinning counter electrode. Partially oriented NWs along the aligned electrospun fibers enabled us to develop a highly oriented 1D structure over a large ($cm^2$ scale) area. The degree of linear polarization of the aligned composite fibers showed a 76% improvement compared to that of the NW/DCM dispersion. This method can be applied to different all-inorganic halide perovskites such as $CsPbI_3$ to further enhance the polarization of the composite system. This hierarchical structure can potentially be used in optical devices such as displays that require polarized light emission from a solid film. However, the stability of these all-inorganic perovskites in organic solvents as well as polymer matrices remains an issue.

## Acknowledgments

MMD acknowledges the 'Outstanding Young Investigator' grant of the Turkish Academy of Sciences (TÜBA-GEBİP 2013).

**Author contributions**

This manuscript was written with contributions from all authors. All authors have approved the final version of the manuscript.

## ORCID iDs

Mustafa M Demir https://orcid.org/0000-0003-1309-3990

## References

[1] Li X, Cao F, Yu D, Chen J, Sun Z, Shen Y, Zhu Y, Wang L, Wei Y and Wu Y 2017 All inorganic halide perovskites nanosystem: synthesis, structural features, optical properties and optoelectronic applications *Small* **13** 1603996

[2] Song J, Li J, Li X, Xu L, Dong Y and Zeng H 2015 Quantum dot light-emitting diodes based on inorganic perovskite cesium lead halides ($CsPbX_3$) *Adv. Mater.* **27** 7162–7

[3] Beal R E, Slotcavage D J, Leijtens T, Bowring A R, Belisle R A, Nguyen W H, Burkhard G F, Hoke E T and McGehee M D 2016 Cesium lead halide perovskites with improved stability for tandem solar cells *J. Phys. Chem. Lett.* **7** 746–51

[4] Nedelcu G, Protesescu L, Yakunin S, Bodnarchuk M I, Grotevent M J and Kovalenko M V 2015 Fast anion-exchange in highly luminescent nanocrystals of cesium lead halide perovskites ($CsPbX_3$, X = Cl, Br, I) *Nano Lett.* **15** 5635–40

[5] Swarnkar A, Chulliyil R, Ravi V K, Irfanullah M, Chowdhury A and Nag A 2015 Colloidal $CsPbBr_3$ perovskite nanocrystals: luminescence beyond traditional quantum dots *Angew. Chem. Int. Ed.* **127** 15644–8

[6] Hoffman J B, Schleper A L and Kamat P V 2016 Transformation of sintered $CsPbBr_3$ nanocrystals to cubic $CsPbI_3$ and gradient $CsPbBr_xI_{3-x}$ through halide exchange *J. Am. Chem. Soc.* **138** 8603–11

[7] Amgar D, Stern A, Rotem D, Porath D and Etgar L 2017 Tunable length and optical properties of $CsPbX_3$ (X = Cl, Br, I) nanowires with a few unit cells *Nano Lett.* **17** 1007–13

[8] Guhrenz C, Benad A, Ziegler C, Haubold D, Gaponik N and Eychmüller A 2016 Solid-state anion exchange reactions for color tuning of $CsPbX_3$ perovskite nanocrystals *Chem. Mater.* **28** 9033–99040

[9] Akkerman Q A, D'Innocenzo V, Accornero S, Scarpellini A, Petrozza A, Prato M and Manna L 2015 Tuning the optical properties of cesium lead halide perovskite nanocrystals by anion exchange reactions *J. Am. Chem. Soc.* **137** 10276–81

[10] Ramasamy P, Lim D-H, Kim B, Lee S-H, Lee M-S and Lee J-S 2016 All-inorganic cesium lead halide perovskite nanocrystals for photodetector applications *Chem. Commun.* **52** 2067–70

[11] Wang Y, Li X, Song J, Xiao L, Zeng H and Sun H 2015 All-inorganic colloidal perovskite quantum dots: a new class of lasing materials with favorable characteristics *Adv. Mater.* **27** 7101–8

[12] Zhang Q, Su R, Liu X, Xing J, Sum T C and Xiong Q 2016 High-quality whispering-gallery-mode lasing from cesium lead halide perovskite nanoplatelets *Adv. Funct. Mater.* **26** 6238–45

[13] Wang Y, Li X, Nalla V, Zeng H and Sun H 2017 Solution-processed low threshold vertical cavity surface emitting lasers from all-inorganic perovskite nanocrystals *Adv. Funct. Mater.* **27** 1605088

[14] Yakunin S, Protesescu L, Krieg F, Bodnarchuk M I, Nedelcu G, Humer M, De Luca G, Fiebig M, Heiss W and Kovalenko M V 2015 Low-threshold amplified spontaneous emission and lasing from colloidal nanocrystals of caesium lead halide perovskites *Nature Commun.* **6** 8056

[15] Li G, Rivarola F W R, Davis N J, Bai S, Jellicoe T C, de la Peña F, Hou S, Ducati C, Gao F and Friend R H 2016 Highly efficient perovskite nanocrystal light-emitting diodes enabled by a universal crosslinking method *Adv. Mater.* **28** 3528–34

[16] Yassitepe E, Yang Z, Voznyy O, Kim Y, Walters G, Castañeda J A, Kanjanaboos P, Yuan M, Gong X and Fan F 2016 Amine-free synthesis of cesium lead halide perovskite quantum dots for efficient light-emitting diodes *Adv. Funct. Mater.* **26** 8757–63

[17] Li J, Xu L, Wang T, Song J, Chen J, Xue J, Dong Y, Cai B, Shan Q and Han B 2016 50-Fold EQE improvement up to 6.27% of solution-processed all-inorganic perovskite $CsPbBr_3$ QLEDs via surface ligand density control *Adv. Mater.* **29** 1603885

[18] Goldstein D H 2016 *Polarized Light.* (Boca Raton, FL: CRC Press)

[19] Wang D, Wu D, Dong D, Chen W, Hao J, Qin J, Xu B, Wang K and Sun X 2016 Polarized emission from $CsPbX_3$ perovskite quantum dots *Nanoscale* **8** 11565–70

[20] Akkerman Q A, Motti S G, Kandada A R S, Mosconi E, D'Innocenzo V, Bertoni G, Marras S, Kamino B A, Miranda L and De Angelis F 2016 Solution synthesis approach to colloidal cesium lead halide perovskite nanoplatelets with monolayer-level thickness control *J. Am. Chem. Soc.* **138** 1010–6

[21] Zhang D, Eaton S W, Yu Y, Dou L and Yang P 2015 Solution-phase synthesis of cesium lead halide perovskite nanowires *J. Am. Chem. Soc.* **137** 9230–3

[22] Zhang D, Yang Y, Bekenstein Y, Yu Y, Gibson N A, Wong A B, Eaton S W, Kornienko N, Kong Q and Lai M 2016 Synthesis of composition tunable and highly luminescent cesium lead halide nanowires through anion-exchange reactions *J. Am. Chem. Soc.* **138** 7236–9

[23] Shamsi J, Dang Z, Bianchini P, Canale C, Stasio F D, Brescia R, Prato M and Manna L 2016 Colloidal synthesis of quantum confined single crystal $CsPbBr_3$ nanosheets with lateral size control up to the micrometer range *J. Am. Chem. Soc.* **138** 7240–3

[24] Cunningham P D, Souza J O B Jr, Fedin I, She C, Lee B and Talapin D V 2016 Assessment of anisotropic semiconductor nanorod and nanoplatelet heterostructures with polarized emission for liquid crystal display technology *ACS Nano* **10** 5769–81

[25] Liu L, Huang S, Pan L, Shi L J, Zou B, Deng L and Zhong H 2017 Colloidal synthesis of $CH_3NH_3PbBr_3$ nanoplatelets with polarized emission through self-organization *Angew. Chem. Int. Ed.* **56** 1780–3

[26] Pan A, He B, Fan X, Liu Z, Urban J J, Alivisatos A P, He L and Liu Y 2016 Insight into the ligand-mediated synthesis of colloidal $CsPbBr_3$ perovskite nanocrystals: the role of organic acid, base, and cesium precursors *ACS Nano* **10** 7943–54

[27] Demir M M, Yilgor I, Yilgor E and Erman B 2002 Electrospinning of polyurethane fibers *Polymer* **43** 3303–9

[28] Molenkamp W C, Watanabe M, Miyata H and Tolbert S H 2004 Highly polarized luminescence from optical quality films of a semiconducting polymer aligned within oriented mesoporous silica *J. Am. Chem. Soc.* **126** 4476–7

[29] Nguyen T-Q, Wu J, Doan V, Schwartz B J and Tolbert S H 2000 Control of energy transfer in oriented conjugated polymer-mesoporous silica composites *Science* **288** 652–6

[30] Demir M M, Ozen B and Özçelik S. 2009 Formation of pseudoisocyanine J-aggregates in poly (vinyl alcohol) fibers by electrospinning *J. Phys. Chem.* B **113** 11568–73

[31] Li D, Wang Y and Xia Y 2003 Electrospinning of polymeric and ceramic nanofibers as uniaxially aligned arrays *Nano Lett.* **3** 1167–71

[32] Doshi J and Reneker D H 1995 Electrospinning process and applications of electrospun fibers *J. Electrostat.* **35** 151–60

[33] Yaman M, Khudiyev T, Ozgur E, Kanik M, Aktas O, Ozgur E O, Deniz H, Korkut E and Bayindir M 2011 Arrays of indefinitely long uniform nanowires and nanotubes *Nature Mater.* **10** 494–501

[34] Yan W, Qu Y, Gupta T D, Darga A, Nguyên D T, Page A G, Rossi M, Ceriotti M and Sorin F 2017 Semiconducting nanowire-based optoelectronic fibers *Adv. Mater.* **29** 1700681

[35] Horzum N, Muñoz-Espí R, Glasser G, Demir M M, Landfester K and Crespy D 2012 Hierarchically structured metal oxide/silica nanofibers by colloid electrospinning *ACS Appl. Mater. Inter.* **4** 6338–45

[36] Demir M M, Horzum N, Özen B and Özçelik S 2013 Hierarchial coassembly of a cyanine dye in poly (vinyl alcohol) fibrous films by electrospinning *J. Phys. Chem.* B **117** 10920–8

[37] Demir M M, Soyal D, Ünlü C, Kuş M and Özçelik S 2009 Controlling spontaneous emission of CdSe nanoparticles dispersed in electrospun fibers of polycarbonate urethane *J. Phys. Chem.* C **113** 11273–8

[38] Cottingham P and Brutchey R L 2016 On the crystal structure of colloidally prepared $CsPbBr_3$ quantum dots *Chem. Commun.* **52** 5246–9

[39] Raja S N, Bekenstein Y, Koc M A, Fischer S, Zhang D, Lin L, Ritchie R O, Yang P and Alivisatos A P 2016 Encapsulation of perovskite nanocrystals into macroscale polymer matrices: enhanced stability and polarization *ACS Appl. Mater. Inter.* **8** 35523–33

[40] Hikmet R A, Chin P T, Talapin D V and Weller H 2005 Polarized-light-emitting quantum-rod diodes *Adv. Mater.* **17** 1436–9

[41] Higgins C, Lunz M, Bradley A L, Gerard V A, Byrne S, Gun'ko Y K, Lesnyak V and Gaponik N 2010 Energy transfer in colloidal CdTe quantum dot nanoclusters *Opt. Express* **18** 24486–94

[42] Kagan C, Murray C, Nirmal M and Bawendi M 1996 Electronic energy transfer in CdSe quantum dot solids *Phys. Rev. Lett.* **76** 1517–20

[43] Chappell H E, Hughes B K, Beard M C, Nozik A J and Johnson J C 2011 Emission quenching in PbSe quantum dot arrays by short-term air exposure *J. Phys. Chem. Lett.* **2** 889–93

[44] Nair G, Geyer S M, Chang L-Y and Bawendi M G 2008 Carrier multiplication yields in PbS and PbSe nanocrystals measured by transient photoluminescence *Phys. Rev.* B **78** 125325

[45] Zhang H, Hu B, Sun L, Hovden R, Wise F W, Muller D A and Robinson R D 2011 Surfactant ligand removal and rational fabrication of inorganically connected quantum dots *Nano Lett.* **11** 5356–61